AIP | Applied Physics Letters

A Maxwell's fish eye lens for the terahertz region

Jingbo Liu, Rajind Mendis, and Daniel M. Mittleman

Citation: Appl. Phys. Lett. **103**, 031104 (2013); doi: 10.1063/1.4813820
View online: http://dx.doi.org/10.1063/1.4813820
View Table of Contents: http://apl.aip.org/resource/1/APPLAB/v103/i3
Published by the AIP Publishing LLC.

A Maxwell's fish eye lens for the terahertz region

Jingbo Liu, Rajind Mendis, and Daniel M. Mittleman
Department of Electrical and Computer Engineering, MS-378, Rice University, Houston, Texas 77005, USA

(Received 21 May 2013; accepted 26 June 2013; published online 15 July 2013)

We implement a two-dimensional Maxwell's fish eye lens using a waveguide-based artificial dielectric. The Maxwell's fish eye lens consists of two metallic cylindrical plates sandwiching a free-space region, with the inner surface of one plate shaped into a hollow conical form. This lens has the capability to image terahertz beams from a source located at the edge (between the plates) to the diametrically opposite point on the edge, independent of the incident angle. © *2013 AIP Publishing LLC*. [http://dx.doi.org/10.1063/1.4813820]

A gradient index (GRIN) lens is an example of an optical device whose focusing effect is realized by a spatial variation of the refractive index of the constituent material.[1] The design and fabrication of devices like GRIN lenses using naturally occurring dielectric media has been an on-going challenge, particularly at long wavelengths, since traditional approaches such as continuously varying doping,[2] are not practical. In the far infrared and beyond, it has been difficult to achieve a continuously varying index in bulk optical components. Some fabrication methods have been explored to approximately emulate the gradient index, such as the onion-shell technique,[3] the tapered hole approach,[4] and the slice technique.[5] These approaches roughly approximate the gradient index, but each suffers from various aberrations due to the non-ideal index variation. The emerging disciplines of metamaterials[6–9] and artificial dielectrics[10–12] have opened up several possibilities to realize devices with spatially varying dielectric parameters. Here, using artificial dielectrics, we implement a GRIN device with an ideal, continuously varying index distribution.

The Maxwell's fish eye (MFE) lens[13,14] is one example of a GRIN device that has recently attracted a great deal of interest.[15–19] The MFE lens is a spherically symmetrical lens with the refractive index conforming to the equation

$$n(r) = \frac{n_0}{1 + (r/R)^2}, \tag{1}$$

where n_0 is a constant, R is the radius of the sphere, and r is the radial distance from the center. Designed on the basis of geometrical optics, the MFE lens can image light rays emitted from a point source on the spherical surface to the diametrically opposite point on the surface. The unique focusing and imaging properties of the MFE lens have recently been exploited to design a dielectric antenna.[18] Moreover, it has been suggested, somewhat controversially, that an ideal MFE constitutes a perfect lens whose resolution is not limited by the wavelength.[15–17,20,21]

In the terahertz (THz) range, it is possible to construct a nearly ideal GRIN device using waveguide-based artificial dielectrics.[10–12] When a parallel-plate waveguide (PPWG) is excited to operate in the TE_1 mode, the free-space region between the metal plates has an effective index of refraction given by

$$n = \sqrt{1 - (c/2bf)^2}, \tag{2}$$

where b is the plate separation, c is the speed of light in free-space, and f is the frequency. At a given frequency f greater than the TE_1-mode cutoff frequency $f_c = c/2b$, the index of refraction can have any value in the range between 0 and 1, by adjusting the plate separation of the PPWG.[12] Moreover, this effective refractive index can be engineered to vary almost arbitrarily in the two-dimensional (2D) space defined by the two metal plates, simply by slowly varying the plate separation b. In this study, we report a 2D version of a MFE lens implemented using this concept.

In the traditional MFE lens, the index of refraction has a spherically symmetric radial variation from $n = 2$ in the center to $n = 1$ on the surface. In this case, the constant n_0 in Eq. (1) is 2, and since the refractive index on the surface matches that of free space, waves couple in and out of the lens without any reflections. However, this index-matching is not essential to the focusing properties of the MFE lens. We conduct a 2D ray-tracing simulation to validate this focusing capability [Fig. 1(a)]. The refractive index inside a circle of radius 2.5 cm is set according to Eq. (1) with $n_0 = 0.9$. On the circumference of the circle, the index of refraction is 0.45. As expected, light rays emitted from a point source on the circumference of the circle are focused exactly to the diametrically opposite point.

To implement this MFE lens, we fabricate a waveguide consisting of two circular metal plates in which the plate spacing varies radially. Combing Eqs. (1) and (2), the plate separation b can be derived as a function of the distance to the center (r) as

$$b(r) = \frac{\lambda}{2} \frac{1}{\sqrt{1 - \left[\frac{n_0}{1 + (r/R)^2}\right]^2}}. \tag{3}$$

Here, λ is the wavelength at the design frequency. For this demonstration, we choose a design frequency of 0.15 THz ($\lambda = 2$ mm), and $n_0 = 0.9$ and $R = 2.5$ cm, as above. The bottom plate has a flat inner surface, while the top plate has a hollow conical inner surface. The curvature of the top surface is specified in such a way that when the two plates are held adjacent to each other the plate separation varies according to Eq. (3) [Fig. 1(b)].

In fabricating the device, the bottom plate is made of aluminum by conventional machining. To fabricate the top (non-uniform) plate, we employ a high-resolution 3D

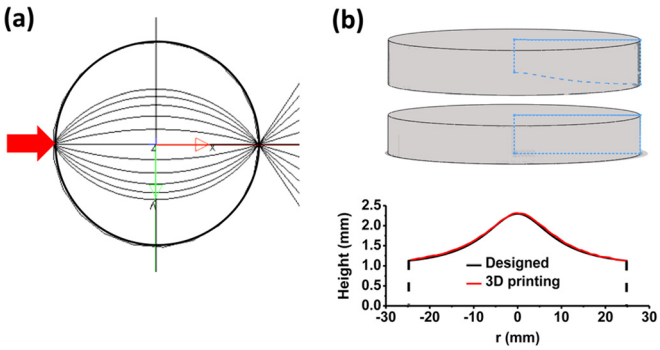

FIG. 1. (a) Ray-tracing simulation of the 2D Maxwell's fish eye lens. (b) The profile of the cross-section of the MFE lens. The red solid curve is the measured profile of the top plate made by 3D printing, while the black solid curve is the designed curve according to Eq. (3).

printing technique,[22] which produces an accurate finish with a resolution of better than 25 μm. The fabrication was carried out by a commercial vendor using a PolyJet 3D printer. The plot in Fig. 1(b) shows the measured (via digital image processing) surface profile of the fabricated waveguide (red curve), which overlaps very well with the theoretical design curve (black curve). Then, we coat the curved surface of the plastic plate with a $\sim$20 μm-thick layer of high-conductivity paint (MG Chemicals 841 Super Shield Nickel Conductive Coating). The conductivity of the paint is as high as that of nickel, and the roughness of the painted surface is much less than the design wavelength. Therefore, the metal-coated surface of the top plate behaves as a smooth bulk metal and can serve as the upper plate of our waveguide-based MFE lens.

The experimental setup to investigate the imaging properties of the MFE lens is shown in Fig. 2(b). We use a fiber-coupled THz time-domain-spectroscopy (TDS) system, which generates THz pulses consisting of frequencies ranging from about 0.05 THz to almost 2 THz. In order to excite the TE_1 mode in the lens, the polarization of the incident THz beam is aligned parallel to the flat surface of the bottom plate. The width of the input beam size was limited at the source point of the MFE lens using a 2 mm slit-aperture. In order to map the output beam profile of the lens, we use a 1 mm slit-aperture in contact with the edge of the MFE lens on the output side, aligned with a set of confocal lenses and

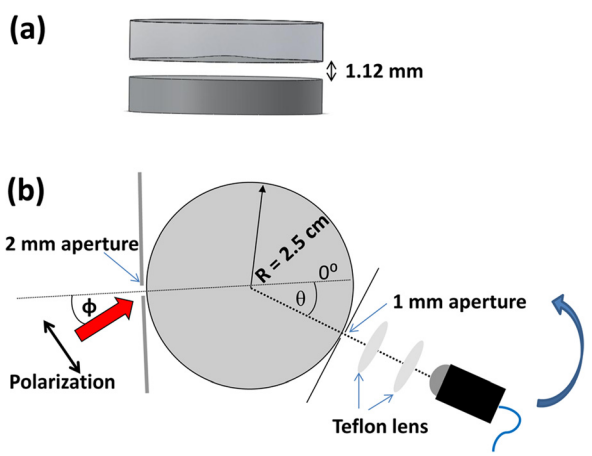

FIG. 2. (a) Horizontal view of the assembled MFE lens used in the experiment. (b) The top view of the experimental setup.

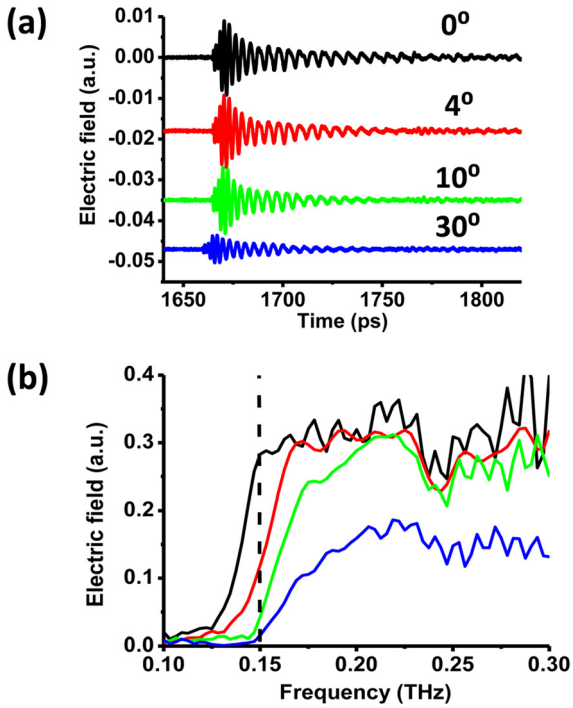

FIG. 3. (a) Typical time-domain signals at different scan angles along the circumference of the lens on the output side of the lens. (b) Corresponding amplitude spectra.

the THz receiver. This optical configuration effectively images the THz signal at the edge of the lens to the THz receiver, so the resolution of the measurement is determined by the aperture size ($\sim$1 mm). We scan the aperture together with the receiver optics along the circumference of the MFE lens. The scan ranges from about $-45°$ to about $+45°$ with a step size of 2°. The 0° reference is located at the diametrically opposite point to the input aperture.

Typical time domain signals are shown in Fig. 3(a) for various angular positions. The 0° reference angle also corresponds to the expected focal spot of the MFE lens. The time domain signals exhibit a negative chirp, characteristic of the TE_1 mode.[23] To collect all the spectral information, we used a reasonably long time window (150 ps) in the Fourier-transform analysis. Figure 3(b) gives the amplitude spectra corresponding to the time signals in Fig. 3(a). At the design frequency of 0.15 THz, we observe a sharp drop in the

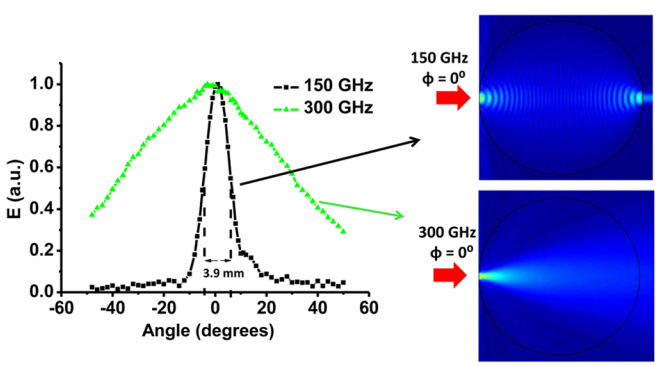

FIG. 4. Measured electric field as a function of the scan angle for 0.15 THz (design frequency) and 0.3 THz. The FWHM of the focal spot at 0.15 THz is 3.9 mm. The top and bottom insets are FEM simulations corresponding to 0.15 THz and 0.3 THz, respectively.

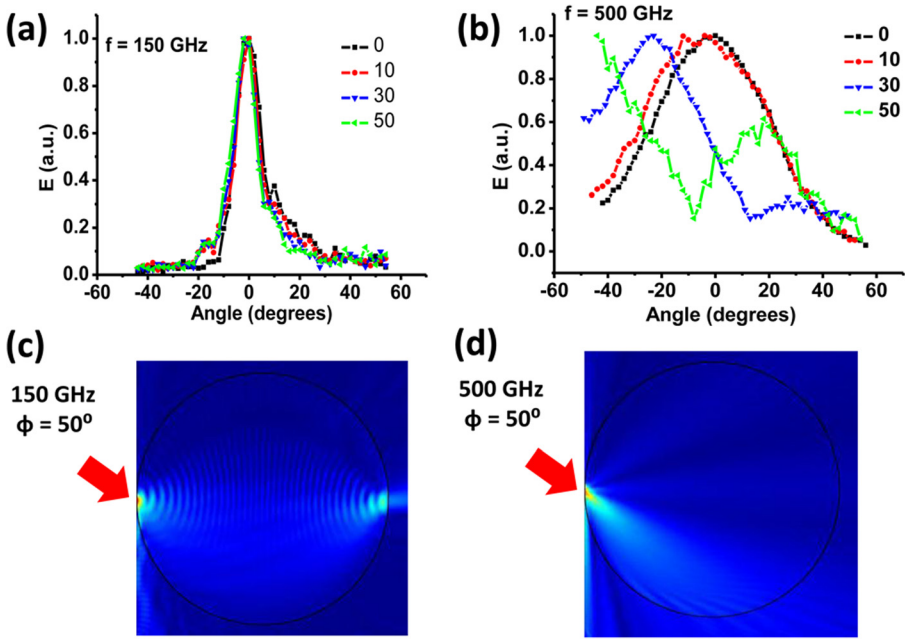

FIG. 5. (a) Measured electric field as a function of scan angle for a frequency of 0.15 THz and incident angles of 0°, 10°, 30°, and 50°. (b) Measured electric field as a function of scan angle for a frequency of 0.5 THz and incident angles of 0°, 10°, 30°, and 50°. (c) FEM simulation for an incident angle of 50° and a frequency of 0.15 THz. (d) FEM simulation for an incident angle of 50° and a frequency of 0.5 THz.

amplitude when the receiver scans from 0° to 4°, compared to the amplitude changes at the other frequencies. The amplitude at 0.15 THz drops to almost zeros when the receiver scan angle exceeds 10°. This sharp drop of the signal at 0.15 THz is a manifestation of the focusing effect of MFE lens at its design frequency.

The focusing effect is more prominent in Fig. 4, where we have extracted the field amplitude at the frequencies of 0.15 THz and 0.3 THz and plotted them as a function of the scan angle. For comparison, the profile at each frequency is normalized to the peak value. At the design frequency of 0.15 THz, the MFE shows a good focal spot having a full-width-at-half-maximum (FWHM) of 3.9 mm (note that an angle of 1° corresponds to an arc-length of 0.44 mm on the lens circumference). At the higher frequency of 0.3 THz, the beam is highly diffracted due to the relatively small input aperture. These results are consistent with 3D numerical simulations (shown in the inset of Fig. 4) based on the finite-element method (FEM).[24] We note that in the simulation we assume that the operating mode of the MFE lens is a pure TE_1 mode, but a pure TE_1 mode is very difficult to achieve experimentally, due to the inherent mode mismatch at the input to the lens.[23] A certain amount of the input energy will be coupled to the higher-order TE_3 mode. This probably explains the relatively larger size of the measured focal spot of 3.9 mm, which is almost twice the size of the input aperture.

We further characterize the MFE by changing the incident beam angle (Φ). The MFE lens is predicted to image light emitted from a point source to the same output point, regardless of the incident angle.[13,14] We varied the incident angle Φ of the input THz beam from 0° to 50° and made the same angular measurement for each incident angle. The results are shown in Fig. 5. As expected, the focal-spot profiles are virtually the same at a frequency of 0.15 THz, for all the incidence angles, as shown in Fig. 5(a). The FWHM of the profile is 4 mm for the incident angle of 50°, which is almost the same as that of 0° incidence. In comparison, the beams at higher frequencies are less influenced by the MFE lens. The higher the frequency, the less the MFE lens affects the wave propagation. Figure 5(b) shows the profiles of the signals at a frequency of 0.5 THz. We observe that when the incident angle increases, the profile experiences relatively the same angular shift. The angular shift at the high frequency and the imaging effect at the design frequency are confirmed by FEM simulations [Figs. 5(c) and 5(d), respectively].

In summary, we have implemented a Maxwell's fish eye lens with an ideal (non-discretized) index gradient based on a 2D inhomogeneous artificial dielectric medium. This 2D MFE lens works at a specifically chosen design frequency of 0.15 THz and has the capability to image THz radiation from a source located at a point on its surface to the diametrically opposite point, regardless of the incident angle. This device could have important applications in the design of wide-angle THz detectors. Therefore, the use of waveguide-based inhomogeneous artificial dielectrics as the basis for GRIN optics offers an effective technology for the realization of THz optical components with unique and valuable properties.

[1]E. Hecht, *Optics* (Addison-Wesley, 2001).
[2]C. Gomez-Reino, M. V. Perez, and C. Bao, *Gradient-Index Optics: Fundamentals and Applications* (Springer, 2010).
[3]G. D. M. Peeler and H. P. Coleman, IRE Trans. Antennas Propag. **6**, 202 (1958).
[4]K. A. Zimmerman and D. L. Runyon, U.S. patent 5,677,796 (1997).
[5]S. Rondineau, M. Himdi, and J. Sorieux, IEEE Antennas Wireless Propag. Lett. **2**, 163 (2003).
[6]R. A. Shelby, D. R. Smith, S. C. Nemat-Nasser, and S. Schultz, Appl. Phys. Lett. **78**, 489 (2001).
[7]D. R. Smith, J. B. Pendry, and M. C. K. Wiltshire, Science **305**, 788 (2004).
[8]V. M. Shalaev, W. Cai, U. K. Chettiar, H.-K. Yuan, A. K. Sarychev, V. P. Drachev, and A. V. Kildishev, Opt. Lett. **30**, 3356 (2005).
[9]J. Valentine, S. Zhang, T. Zentgraf, E. Ulin-Avila, D. A. Genov, G. Bartal, and X. Zhang, Nature (London) **455**, 376 (2008).
[10]R. Mendis and D. M. Mittleman, IEEE Trans. Microwave Theory Tech. **58**, 1993 (2010).
[11]R. Mendis, A. Nag, F. Chen, and D. M. Mittleman, Appl. Phys. Lett. **97**, 131106 (2010).

[12]R. Mendis, J. Liu, and D. M. Mittleman, Appl. Phys. Lett. **101**, 111108 (2012).
[13]J. C. Maxwell, Camb. Dublin Math J. **8**, 188 (1853).
[14]C. T. Tai, Nature (London) **182**, 1600 (1958).
[15]U. Leonhardt, New J. Phys. **11**, 093040 (2009).
[16]Y. G. Ma, S. Sahebdivan, C. K. Ong, T. Tyc, and U. Leonhardt, New J. Phys. **13**, 033016 (2011).
[17]U. Leonhardt and T. G. Philbin, Phys. Rev. A **81**, 011804 (2010).
[18]B. Fuchs, O. Lafond, S. Rondineau, and M. Himdi, IEEE Trans. Microwave Theory Tech. **54**, 2292 (2006).
[19]V. N. Smolyaninova, I. I. Smolyaninov, A. V. Kildishev, and V. M. Shalaev, Opt. Lett. **35**, 3396 (2010).
[20]T. Tyc and X. Zhang, Nature (London) **480**, 42 (2011).
[21]R. Merlin, J. Opt. **13**, 024017 (2011).
[22]Z. Wu, W. Ng, M. E. Gehm, and H. Xin, Opt. Express **19**, 3962 (2011).
[23]R. Mendis and D. M. Mittleman, Opt. Express **17**, 14839 (2009).
[24]J. Deibel, M. Escarra, N. Berndsen, K. Wang, and D. M. Mittleman, Proc. IEEE **95**, 1624 (2007).